CHAPTER – 1

Introduction
and
Literature Review

CHAPTER 1

INTRODUCTION AND LITERATURE REVIEW

1.1 Historical sketch

The anthropologists often define human civilization based on the materials in relevance during those eras. The surge to fulfil humankind's ever-evolving need has led to the accidental discovery of many metals, materials, and alloys. The development of rudimentary techniques like smelting has led to the inception of copper (5000 BC) from its ore, and its accidental alloying with tin has given birth to bronze (3500 BC). This addition of alloying elements into the base metal has led to a significant increase in strength of the alloy compared to that of monolithic metals. The art of alloying may be considered as one of the greatest gift, that metallurgy has extended to humanity. This led to the development of various types of steel, an alloy of iron and carbon (1850 onwards), light metals (the 1940s), and other technologically advanced special alloys. The science of alloy design and development further gained impetus with optical metallographic techniques in the 20^{th} century. This helped establish the correlation between the microstructure and properties of newly designed alloys. These new materials have brought a paradigm shift in the transportation industry, aerospace and defence sector, and many other sectors. In the late 20^{th} century, a new class of material known as metal matrix composite was designed by reinforcing secondary phases in monolithic metals and alloys for enhancing their properties.

Besides the modern engineering alloys and composites, several novel materials like intermetallics, quasicrystals, metallic glasses, and high-entropy alloys were also developed by persistent efforts of the researchers throughout the globe. Intermetallic compounds, in general, comprise two or more metallic elements and the crystal structure are different from the base metals. The high-temperature strength and stability of these intermetallic compounds have attracted the interest of scientific community as a material for high

temperature applications. The inherent room temperature brittleness of intermetallic compounds restrict its usage as a structural material. However, its properties like high hardness, low coefficient of friction, etc., may be exploited as reinforcement in metal matrix composites and as suitable material for coating applications. In the year 1982, Shechtman observed a forbidden fivefold rotation symmetry in Al – Mn alloys and it was in 1984, giving rise to the concept of quasicrystal [1]. The breakthrough experiment conducted by Shechtman et al. [1] brought a paradigm shift in the conventional crystallographic concepts for which he was awarded the Noble Prize in the year 2011 to discover quasicrystals.

The alloys discussed till the point have 2–3 major elements. However, Brian Cantor from Oxford University explored the possibility of developing a single-phase solid solution by equiatomic multicomponent alloys having five or more than five elements [2]. He, along with his undergraduate student, has reported the formation of a single-phase solid solution in CoCrFeMnNi (at%) having FCC structure. In parallel to this, another group in Taiwan under J W Yeh also independently reported the formation of single-phase solid solutions in many equiatomic multicomponent alloy compositions [3]. J W Yeh coined the term high entropy alloys (HEAs) with five or more elements, having a composition in elements greater than 5% and less than 35%, and the entropy mixing entropy (i.e., configurational entropy) greater than 1.5R.

1.2 Quasicrystalline materials

In the year 1984, with the discovery of quasicrystal (QC) in Al-Mn alloy by Dan Shechtman, a new class of aperiodic crystals came into existence, changing the concept of conventional crystallography [1]. They have used rapid solidification to synthesize Al–14(at %) Mn, have long-range order without translational periodicity, and have forbidden rotational symmetry. These alloys have non-periodic atomic arrangements exhibiting sharp diffraction peaks with icosahedral symmetry. It was confirmed that Al-Mn rapidly

quenched alloy does not have any sign of twinning through transmission electron microscopy.

The twinning in crystalline materials sometimes leads to icosahedral symmetry, usually observed in the case of gold. The materials with icosahedral point group symmetry lacks translational periodicity. As per the conventional crystallographic concepts, the diffraction peaks sharpness was considered to be due to the periodicity of the crystalline materials. Levine and Steinhardt [4,5] first coined the term 'quasicrystals' after the discovery of the icosahedral phase in Al-Mn alloy and referred to it as icosahedral quasicrystal (IQC). They have simulated the diffraction patterns of quasicrystals having aperiodic lattice in two dimensions (2D) and three-dimension (3D) with icosahedral bond orientation order. They have extended the findings of Penrose [6] and Mackay [7] for filling the space aperiodically by a finite number of tiles in 2D and 3D, respectively. Surprisingly, the simulated diffraction patterns were very close to that observed by Shechtman et al. [1] in Al-Mn alloy through transmission electron microscopy (TEM).

Subsequently, the decagonal quasicrystalline phase was also discovered Chattopadhyay et al. [8] and Bendersky [9] independently in Al-Mn alloys processed through rapid solidification. The decagonal quasicrystals have ten-fold rotational symmetry with quasi-periodicity in two dimensions and periodic arrangement in the third dimension. The dodecagonal quasicrystal having twelve-fold rotational symmetry and quasi-periodicity in two dimensions was first reported by Ishimasa et al. [10] in Ni-70 (at%) Cr alloy prepared by gas evaporation techniques. Similarly, Wang et al. [11] illustrated the presence of two-dimensional quasi-periodicity with eight-fold rotational symmetry in V-Ni-Si and Cr-Ni-Si ternary alloys. After the discovery of 3D and 2D quasicrystals, Chattopadhyay et al. [12] and He et al. [13] reported the presence of 1D quasi-periodicity in Al-Cu-Ni vacancy ordered phases and rapidly solidified Al-Ni-Si alloys, respectively.

In the initial days, almost all the quasicrystals were prepared by rapid solidification and believed to be inherently metastable. It was challenging to prepare single grain samples in a bigger length scale and was limited to micron size. However, the situation does not prevail for long and changed in 1986, with the first illustration of stable icosahedral phase in Al_6Li_3Cu by Dubost et al. [14] by conventional ingot melting. Subsequently, Tsai and co-workers reported the formation of stable quasicrystalline phases in a few Al-transition metal ternary composition, i.e., Al-Cu-Fe [15–17], Al-Cu-Ru [18], Al-Cu-Os [19], Al-Cu-Re [20], Al-Pd-Mn [21], Al-Co-Ni [22] and Al-Cu-Co [22] systems.

In the year 2000, A P Tsai and his co-workers made a significant breakthrough by discovering icosahedral phases in binary Cd-Yb and Ca-Cd systems [23–26]. They have further extended the study on Cd-based ternary quasicrystalline materials by alloying rare earth elements (RE) in Cd-Mg-RE like (RE=Y, Nd, Tb, Dy, Ho, etc.) [25]. A few researchers have also made considerable efforts to develop Cu-based [27,28] and Ti/Zr/Hf based quasicrystalline materials [29–34]. Apart from the quasicrystalline phases reported in the alloy system developed by researchers and co-workers, a few pieces of literature have also shown the existence of naturally occurring quasicrystals [35,36]. As of date, more than 100 different compositions are known to form quasicrystalline phases synthesized by various equilibrium and non-equilibrium processing routes [37–41]. Among the known quasicrystalline composition, ~80% of them contains icosahedral phases, and around ~80% of these icosahedral quasicrystals have Al as the major alloying element [39]. This may be the reason for extensive studies being conducted on Al-based quasicrystalline materials and further exploiting its potential applications.

1.3 Crystallography of quasicrystals

In the conventional crystallographic concept, the arrangement of lattice points in three dimensions is used to define a crystal [37,39,42]. There are only fourteen (14) unique

ways of arranging lattice points in three-dimensional spaces known as Bravais lattices [37,39,42]. The incorporation of the motif at the lattice points further introduces the symmetry elements like rotations. The translational and rotational symmetries applied to '14' Bravais lattices give rise to '230' distinctive arrangements. These '230' distinctive arrangement describing translational and rotational symmetry elements in the structure are defined as space group. The conventional crystal structures are limited to one of these 230 space groups [37,39,42]. In crystalline materials, only two-fold, three-fold, four-fold, and six-fold rotational symmetries are allowed [37,39,42]. A crystal (aligning unit cells in three dimensions) with allowed rotational symmetry and translational periodicity can infinitely fill the space. The n-fold symmetry with $n > 6$ and five-fold symmetry is incompatible with periodicity.

The two-dimensional plane can be packed or filed with triangles, squares, and hexagons without any gaps or overlaps. As per the crystallography, a regular polygon with a vertex angle equal to the integer fraction of 2π is compatible with translational periodicity and rotational symmetry. On the contrary, pentagons with a vertex angle of 108° cannot fill the space in 2D and have an uncovered angular gap of 36° [37,39,42]. The heptagons with a vertex angle of 128°57 are not avoiding the overlapping of the tiles.

During the initial day of its inception, quasicrystal posed two major puzzles to the scientific community, i.e., (i) presence of forbidden rotational symmetry and on the other hand, (ii) long-range order without the translational periodicity [37,39,40,42]. These two issues can be better envisaged, manifesting the sharpness of electron diffraction spots usually associated with crystalline materials having translational periodicity. On the contrary, for glassy phase lagging long-range order, broadened halos are evident. However, in quasicrystals, sharp electron diffraction spots without translational periodicity are discerned [37,39,40,42]. The angle between the electron diffraction spots is 36° ($2\pi/10$).

The distances between the electron diffraction spots are not periodic and are related to each other by golden mean represented by 'τ', where $\tau = \left(\frac{1+\sqrt{5}}{2}\right) = 2cos36° = 1.618\ldots$ [37,39,40,42]. In the standard crystallographic practices, Miller indices with three (3) integers represent a crystallographic plane [37,39,40,42,43]. However, in the case of quasicrystals concept of Miller indices cannot be extended due to the incompatibility of quasicrystals with three-dimensional translational periodicity [37,39,40,42].

The ambiguity in the indexing of aperiodic materials was resolved by projecting the quasi-periodic structure in three dimensions to the higher dimensional space [37,39]. This was affirmed by the projection of a two-dimensional periodic sequence in one dimension yielding an aperiodic sequence [38,44–48]. This envisaged the concept of periodicity in higher dimensional space for three-dimensional quasiperiodic structures (i.e., in six-dimensional space, the icosahedral quasicrystals having three-dimensional quasi-periodicity becomes periodic structure [39].

The 3D quasiperiodic structure can be obtained by projection methods from six-dimensional space in a similar fashion. As six vectors form the center to the regular icosahedron vertices are used to define its structure. Therefore three-dimensional aperiodic sequence can be described as a periodic structure in six-dimensional space [44,49]. Thus, for indexing the diffraction pattern of quasi-periodic structure with icosahedral symmetry, six integer indices are usually used as illustrated by Bancel [49] and Elser [44]. The six independent basic vectors (q_x, q_y, q_z) generated by cyclic permutation of (±1, ±τ, 0), pointing towards the icosahedron's vertices, are used for its indexing. The Bancel's and Elser's indexing scheme can be correlated with each other by considering the vector transformations in 6D and considering the scaling factor difference for calculating the lattice constant [50]. In addition, there is also another indexing scheme followed by J W Cahn [51]. In general, two models, namely the Penrose tiling and quasi-unit cell theory,

explain the quasicrystalline structure having icosahedral, octahedral, decagonal and dodecagonal symmetries.

1.3.1 Penrose tiling

In 1979, Sir Roger Penrose described a model for tiling quasiperiodic plane with two or more unit cells or tiles. These unit cells or tilings are used to fill the space in two/ three-dimensions with specific matching rules [6,52–54]. The most commonly used Penrose tilings encompass fat and thin rhombuses having equal edge length and with angles of 72° and 108°, and 36° and 144°, respectively. These structure can also be generated by projection from higher dimensional space[40].

1.3.2 Quasi – unit cell theory

In, theory the repetition of a single closely packed low energy cluster is used to describe the structure of quasicrystals [43,55–57]. In quasi-unit cell theory, the individual clusters have significantly higher bond strength than the inter-cluster bond [58,59]. This further extends the scope to separate the inter-cluster and intra-cluster bond strength, a deciding parameter for quasi-periodic structure formation. The quasi-unit cell theory also allows the atomic sharing and partial overlapping of clusters.

In the preceding sections, efforts were made to understand the crystallography, structure, and classification of quasicrystals. Quasicrystals possess unique properties such as high hardness, excellent wear resistance with the low value of co-efficient of friction, low electrical and thermal conductivity, and excellent corrosion resistance [60]. These properties make them a potential candidate for engineering applications. The alloying elements often used to synthesize quasicrystals are toxic, costly, and not readily available. Among the investigated stable quasicrystals, the Al–Cu–Fe quasicrystalline alloys are an exception. The ternary Al-Cu-Fe icosahedral quasicrystals have attracted attention due to

their easy availability, lack of toxicity, and budget-friendly cost of alloying elements used [60–63]. However, the inherent room temperature brittleness limits its prospects as structural engineering materials. A brief description will be made of the synthesis, properties, and quasicrystals applications in the upcoming section.

1.4 Al-Cu-Fe quasicrystals

In 1939, Bradley and Goldschmidt, for the first time, reported a new phase in the ternary Al-Cu-Fe alloy system [60]. The peritectic reaction between β-$AlFe_3$ phases and the remaining liquid formed this new phase. This new phase was having a chemical formula close to Al_6Cu_2Fe, having a nominal composition of $Al_{65}Cu_{22.5}Fe_{12.5}$ (at %), and was referred to as the 'ψ' phase [60]. In 1987, while investigating the Al-Cu-Fe ternary alloy system, Tsai et al. [15–17,64,65] discerned that the ψ-phase reported by Bradley and Goldschmidt was indeed having an icosahedral rotational symmetry and fell into the class of 3D quasicrystals.

The Al-based IQC phase having Mackay cluster of atoms usually shows electron to atoms ratio in the range of 1.6 to 1.8, while for the case of Bergman cluster observed in Mg-based QC, is in the range of 2.1 to 2.25 [66–69]. The Al-Cu-Fe quasicrystalline materials usually show face-centered ordering and typically belong to the Mackay icosahedral type cluster [67,70]. It is worth mentioning that Mukhopadhyay et al. [71,72] reported the order-disorder transformations for the first time in Al-Mn icosahedral phase. This was another breakthrough, which brought the concept of face-centered ordering in Al-based quasicrystals and led to such arrangement in a few other systems [73,74].

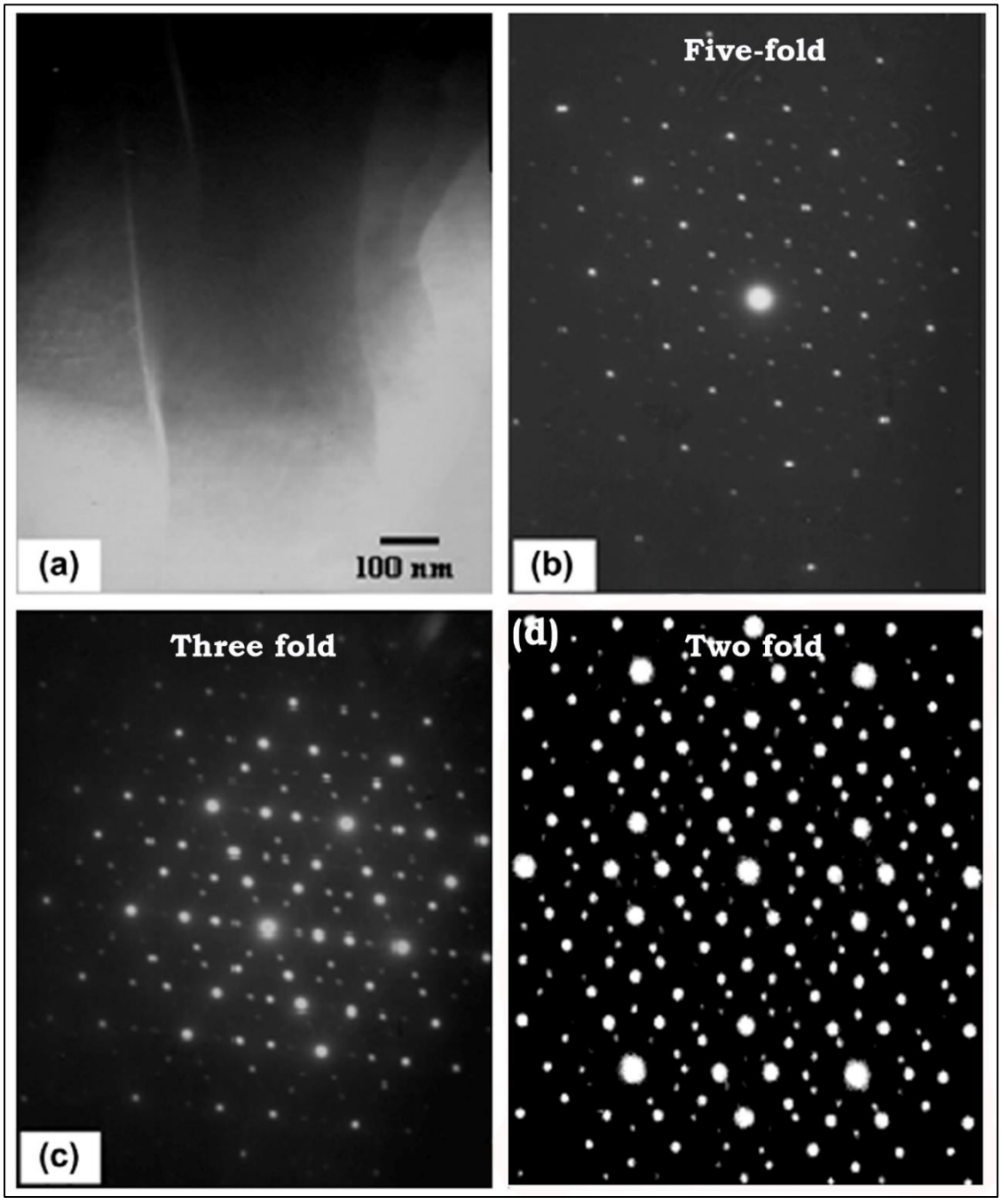

Figure 1. 1: (a) Bright-field image; selected area diffraction (SAD) pattern along (b) five-fold (c) three-fold [75] (d) two-fold axis of rotation in Al-Cu-Fe quasicrystal [76].

The typical electron diffraction pattern can be seen in Figure 1.1, showing the existence of five-, three-, and a two-fold axis of rotation having inflation related to τ. The empirical formulae of important quasicrystalline, approximant, and crystalline phases in the Al-Cu-Fe ternary alloy system are mentioned in Table 1.1.

Table 1. 1: Important binary and ternary phases in Al-Cu-Fe alloy system [60].

Phase	Empirical formula	Crystal structure
ψ	Al_6Cu_2Fe	Icosahedral
λ	$Al_{13}Fe_4$	Monoclinic
ω	Al_7Cu_2Fe	Tetragonal
β	$Al_5(Cu,Fe)_5$, AlFe(Cu)	Cubic (CsCl type)
τ	AlCu(Fe)	Cubic
θ	Al_2Cu	Tetragonal
μ	Al_5Fe_2	Monoclinic

The equilibrium phase diagram with a single quasicrystalline phase for the nominal composition of $Al_{61.75-64}Cu_{25-25.5}Fe_{12-12.75}$ (at %) at room temperature is shown in Figure 1.2 (a). Faudot et al. [77] systematically have shown the compositional range for the presence of a stable single quasicrystalline phase in Al-Cu-Fe alloys (Figure 1.2 (a)). The Al-Cu-Fe alloy systems have a nominal composition of 20 to 28 at % Cu and 10 to 14 at% Fe results in stable quasicrystals. This can be better understood with Figure 1.2 (b) showing the compositional range for the formation of single-phase quasicrystalline material as a function of temperature. It may be inferred from Figure 1.2 (b) that at 860℃ (1133 K), the peritectic reaction among λ_2-Al_3Fe, β-AlFe(Cu), and liquid leads to the formation of icosahedral quasicrystals. A similar kind of observations was also made by Gui et al.[78], studying the formation of the quasicrystalline phase with the composition of $Al_{62}Cu_{25.5}Fe_{12.5}$ (at%). However, they have reported a very narrow compositional range yields stable quasicrystalline phase while annealing in a temperature range of 600℃ (873 K) - 800℃ (1073 K). In contrast to the previous investigation, Yokoyama et al. [79,80] have shown the formation of stable quasicrystalline phase at 820 ℃ (1093 K) by the peritectic reaction between λ_2-Al_3Fe and liquid. They have reported the formation of stable

IQC phase at 40℃ below the temperature observed by Faudot et al. [77]. The study by Yokoyama et al. [79,80] further reports the broad compositional stability of IQC phase in $Al_{65}Cu_{35-x}Fe_x$ (x= 0 – 20 at %) system below the peritectic reaction temperature. However, such broad compositional stability of the IQC phase was not very convincing, because of the previous results showing its stability in a narrow region. During thermally activated processing, the IQC phase in $Al_{65}Cu_{20}Fe_{10}$ (at%) partially transforms into λ-$Al_{13}Fe_4$ to cross the activation energy threshold of ~300 kJ/mol [81]. In an alloy of $Al_{62}Cu_{25.5}Fe_{12.5}$ (at %), the quasicrystalline phase was formed by the peritectic reaction of β-phase and the liquid melt under equilibrium conditions [82]. However, Lee et al. [82] also observed the presence of a minor amount of β-AlFe(Cu), τ-AlCu(Fe), and λ-$Al_{13}Fe_4$ phases along with the major icosahedral quasicrystalline phase. Further, they have shown the effect of annealing temperature on the formation of a stable single-phase IQC. The as-cast Al-Cu-Fe alloy annealed for 3 h at 750 ℃ (973 K) and 850 ℃ (1073 K) led to the formation of a pure IQC phase along with a minor amount of residual β and λ phases respectively. While studying the formation of IQC phase in Al-Cu-Fe alloys with varying composition, Gui et al. [78] made an important observation that the final phases formed after suitable heat treatment are also dependent on the pre-existing crystalline phases in as-cast materials. In general, for Al-Cu-Fe IQC solidified at moderately high and rapidly, it requires no additional annealing treatment; however, some changes in the microstructure might be observed. In a similar context, Holland – Moritz et al. [83] had investigated the effect of solidification rate on Al-Cu-Fe alloys having a nominal composition of $Al_{62}Cu_{25.5}Fe_{12.5}$ (at %) and $Al_{60}Cu_{34}Fe_6$ (at %).

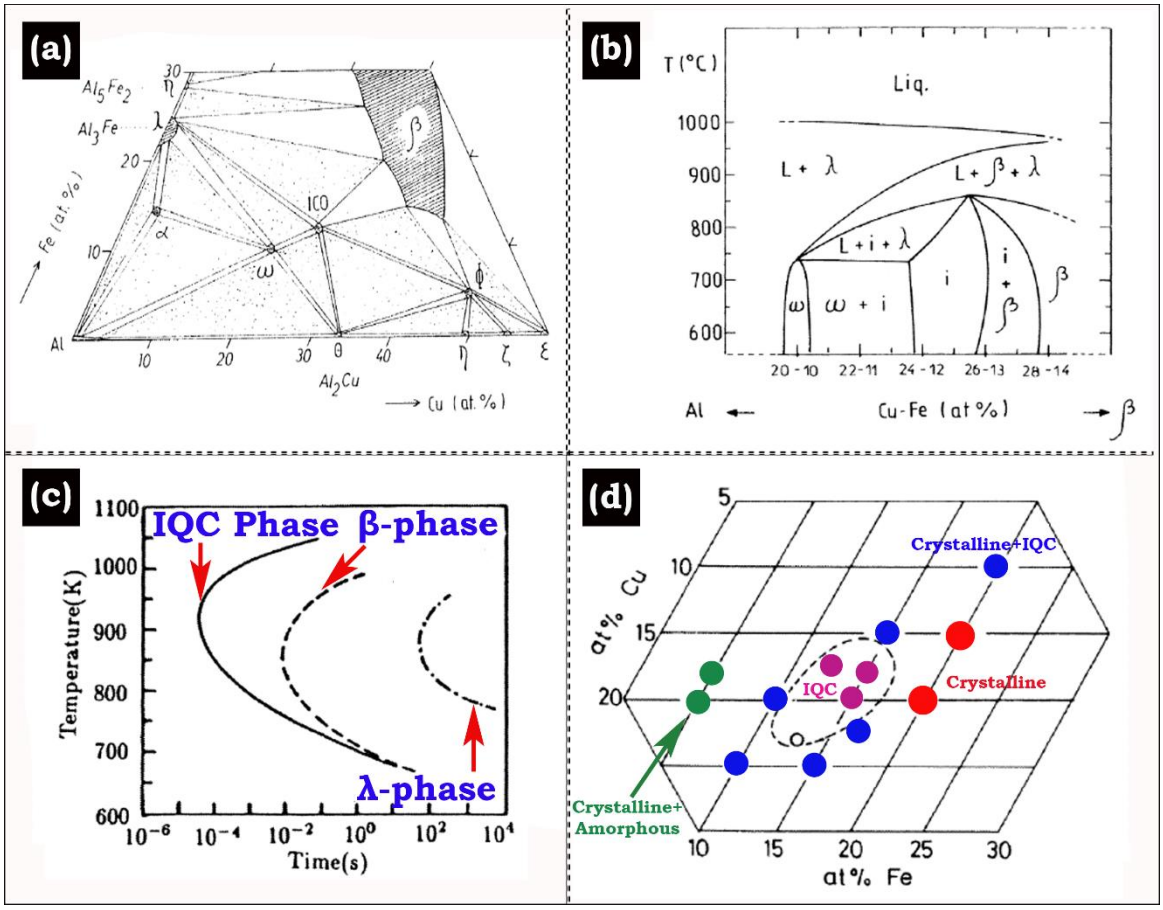

Figure 1. 2: (a) Equilibrium phase diagram depicting the presence of icosahedral and other crystalline phases; (b) pseudo-binary Al-Cu-Fe phase diagram for Al-Cu-Fe IQC showing phases between ω-phase ($Al_{70}Cu_{20}Fe_{10}$) and $Al_{58}Cu_{28}Fe_{14}$ [84]; (c) TTT curve as a function of temperature for Al-Cu-Fe alloy [85]; (d) compositional range for the formation of IQC phases in Al-Cu-Fe alloy by the high cooling rate [15].

During moderate cooling (10^1 – 10^2 °C/s) of $Al_{62}Cu_{25.5}Fe_{12.5}$ (at %) alloy primarily leads to the formation of β and λ phase, followed by peritectic reaction to form the stable IQC phase. Contrary to this, when the cooling rate is high enough (~10^6 °C/s) for $Al_{62}Cu_{25.5}Fe_{12.5}$ (at %), a stable IQC phase can be formed directly. From this observation, it was clear that the processing parameters influence the phases formed after solidification in Al-Cu-Fe alloys [85], as inferred from Figure 1.2 (c). Although the processing conditions strongly affect the phases formed after solidification, the same may be achieved by altering the nominal composition with the processing conditions. The broader stability region for IQC phases in rapidly solidified Al-Cu-Fe alloys can be seen in Figure 1.2 (d).

This shows the desirable composition for the formation of the IQC phase along with other crystalline and amorphous phases.

1.4.1 Synthesis of Al-Cu-Fe quasicrystals

Equilibrium phase diagrams can predict the formation of quasicrystalline and crystalline phases in Al-Cu-Fe alloy systems. It was clear from the phase diagram shown in Figure 1.2 that the conventional melting and solidification processing routes offer a very narrow compositional range for the formation of Al-Cu-Fe based IQC phases [60,86–93] at room temperature. However, to overcome the problem associated with limited compositional range during conventional solidification routes, non-equilibrium processing routes can be employed. The non-equilibrium processing results in metastable quasicrystal formation by widening the solid solubility range and extending the compositional range to form quasicrystals [94]. Several non-equilibrium processing routes, i.e., melt spinning and gas atomization, mechanical alloying, physical vapor deposition and electro-deposition, etc.) can be employed to synthesize quasicrystalline materials, as illustrated in Table 1.2.

Table 1. 2: Non-equilibrium processing routes for the synthesis of quasicrystals [60].

Processing routes / **Parameters**	**Melting and solidification**	**Melt spinning**	**Gas atomization**	**Mechanical alloying**
Thermodynamic stability	Stable	Metastable	Metastable	Metastable
Phase formed	Single-phase IQC generally formed after suitable heat treatment	Single-phase IQC generally formed with and without suitable heat treatment	Single-phase IQC generally formed with and without suitable heat treatment	Single-phase IQC generally formed with and without suitable heat treatment
Desired shape	As per the requirements	Thin ribbons	Powders with particle size ≤150 μm	Fine powder particles with

				layered structure
Quality of QC	Sharp X-ray diffraction peaks; presence of pores if crystalline phases co-exist with IQC phase	Broad X-ray peak due to phasons	Sharp X-ray diffraction peaks	Broad X-ray peak due to phasons; Ordering of IQC may not be complete
Sources of contamination	Air	Air	Air	Air, grinding medium, grinding vessels
Secondary processing	Heat treatment	Compaction or grinding and compaction	Thermal spraying, compaction, sintering, mechanical alloying (heat treatment if desired)	Compaction, sintering, thermal spraying, heat treatment

1.4.1.1 Rapid solidification

The rapid solidification with high cooling rates (~10^6 °C/s) can be achieved through melt spinning or gas atomization to synthesize Al-Cu-Fe IQC alloys. Melt spinning of quasicrystals leads to the formation of a high density of structural defects. These structural defects are also known as phason and understood as the counterpart of defects for crystalline materials. The defect in crystalline materials can be studied through TEM; however, the presence of phasons in quasicrystalline materials can be discerned from the XRD peak broadening. Jono et al. [95] established the stability of the IQC phase in Al-Cu-Fe alloys at high temperatures; however, it decomposes to the crystalline approximant phases during low-temperature annealing. The microstructure of rapidly solidified Al-Cu-Fe IQC alloys are independent of the processing routes employed, i.e., melt spinning or gas

atomization [60]. Even after non-equilibrium processing, melt spinning still yields a stable Al-Cu-Fe IQC phase at room temperature [60].

1.4.1.2 Mechanical alloying

In the past three decades, considerable efforts were made towards synthesizing Al-Cu-Fe IQC alloys through melting and solidification using both equilibrium and non-equilibrium processing routes. However, the narrow composition range and the difference in the density of principal element and the transition elements, i.e., Cu and Fe, offers a considerable challenge for fabricating a stable IQC phase in Al-Cu-Fe ternary system. In contrast to conventional melting and solidification processes, synthesis of nanostructured Al-Cu-Fe IQC through mechanical alloying (MA) routes offers the formation of IQC phases in a broad compositional range Al-Cu-Fe alloys with much less complexity compared to that of the conventional processing routes [96,97,106–113,98–105]. Considerable efforts were made to study the effect of MA on the phase evolution and thermal stability of Al-Cu-Fe IQC. The MA of Al-Cu-Fe elemental powders in the compositional range (in at%) desired for IQC phases leads to the formation of B2-type Al (Cu, Fe) intermetallic and on suitable annealing treatment in the temperature range of 600 ℃ - 800 ℃ leads to the formation of stable IQC phases in Al-Cu-Fe alloys [101,114]. Eckert et al. [115] have reported the appearance of B2-type Al (Cu, Fe) alloys after 70 h of MA with complete dissolution of elemental Cu and minor peaks corresponding to elemental Fe. On further milling, up to 374 h leads to the formation of a B2-type phase with sharp diffraction lines corresponding to homogenous and stable phase appears. The subsequent annealing of the B2-type phase above 600 ℃ leads to a stable IQC phase in Al-Cu-Fe alloys. In another investigation, Srinivas et al. [99,101] reported the formation of the B2-type phase along with minor phases of IQC with the nominal composition of $Al_{70}Cu_{20}Fe_{10}$ (at%). On subsequent annealing at 600 ℃ for four hours of 60 h, mechanically alloyed

B2-type Al (Cu, Fe) + minor IQC phase alloys leads to stable IQC phase along with a minor amount of B2-type phase.

1.4.1.3 Hot pressing and spark plasma sintering

In the past two decades, considerable efforts were made to study the consolidation behavior of Al-based QC and crystalline alloys by non-equilibrium processing like hot pressing [116–118], spark plasma sintering [109,119–124], laser cladding [125], selective laser sintering (SLS) [126,127] and microwave sintering [107,128–130]. Nicula and his co-workers have made considerable efforts in understanding the consolidation behavior of the Al-Cu-Fe IQC phase during SPS [123,128,128,131]. Further, many researchers have made efforts to evaluate the mechanical properties and fracture toughness after non-equilibrium sintering of Al-Cu-Fe IQC alloys having a relative density > 99.00 % [132]. In a detailed investigation, Fleury et al. [132] observed the SPSed Al-Cu-Fe IQC phase having the hardness in the range of 7.75 – 8.90 GPa. The variation of microhardness was dependent on the phases that evolved during the sintering at different temperatures.

1.4.1.4 Coatings of Al-Cu-Fe quasicrystals

The Al-Cu-Fe quasicrystals can be used as an excellent coating material due to the lucrative functional properties. Among the available coating techniques, a few techniques such as plasma and thermal spraying techniques [86,133–136], electron beam coating [137], magnetron sputtering [138–142], cold spraying [143,144], electro-deposition techniques [145], physical vapor deposition [146–149], etc. are used for IQC alloys. However, these coating techniques are encountered with two types of problems (i) depletion of Al in the final composition after coating or film deposition, and (ii) complex peritectic reaction hinders the formation of pure IQC phase and leads to the formation of IQC phase along with other metastable crystalline phases [150–152]. These two challenges

can be handled by tuning the fraction of low melting Al in the IQC composition to overcome the difficulty associated with the depletion of Al during coating or thin film deposition. Further, the stable IQC phases can be developed by additional annealing treatment of coatings or thin films of Al-Cu-Fe alloys.

1.5 Properties of quasicrystals

In the preceding sections, the phase evolution, thermal stability, and synthesis of Al-Cu-Fe quasicrystals were described. Dubois and co-workers have published a few review papers describing the properties and potential application of quasicrystals [153–155]. In the present section, the effect of the phases evolved in Al-Cu-Fe alloys on the physical properties, surface characteristics, and mechanical properties are elaborated.

1.5.1 Physical properties

The electronic properties of quasicrystals are quite different from that of their crystalline counterparts [155]. In general, in the quasicrystalline materials high electrical resistivity is responsible for their low electrical conductivity [156,157]. The studies by Berger et al. [158] have shown the electrical conductivity of Al-Cu-Fe, Al-Pd-Mn, and Al-Pd-Re are in the range corresponding to the doped semiconductors. The electrical resistivity of quasicrystals is having a linear and negative dependence on the temperature, exhibiting electrical conductivity above -243℃ (30 K), particularly for Al-Cu-Fe and Al-Cu-Ru quasicrystals [159,160] as shown in the Figure 1.3 (a). The temperature dependency of a few Al-based quasicrystals is shown in Figure 1.3. Bilusic et al. [161] have established the compositional dependence of quasicrystals on their electrical conductivity. They have demonstrated the higher electrical conductivity for Al-Cu-Fe alloy having a nominal composition of $Al_{63}Cu_{25}Fe_{12}$ (at %) compared to $Al_{62}Cu_{25.5}Fe_{12.5}$ (at %). From this, it may be inferred that the higher Fe content in $Al_{62}Cu_{25.5}Fe_{12.5}$ (at %) quasicrystals decreases the

electrical conductivity due to its proximity with the perfect icosahedral phase [156,161]. The low electrical conductivity may also be attributed to the gap in the conduction band for quasicrystals [162].

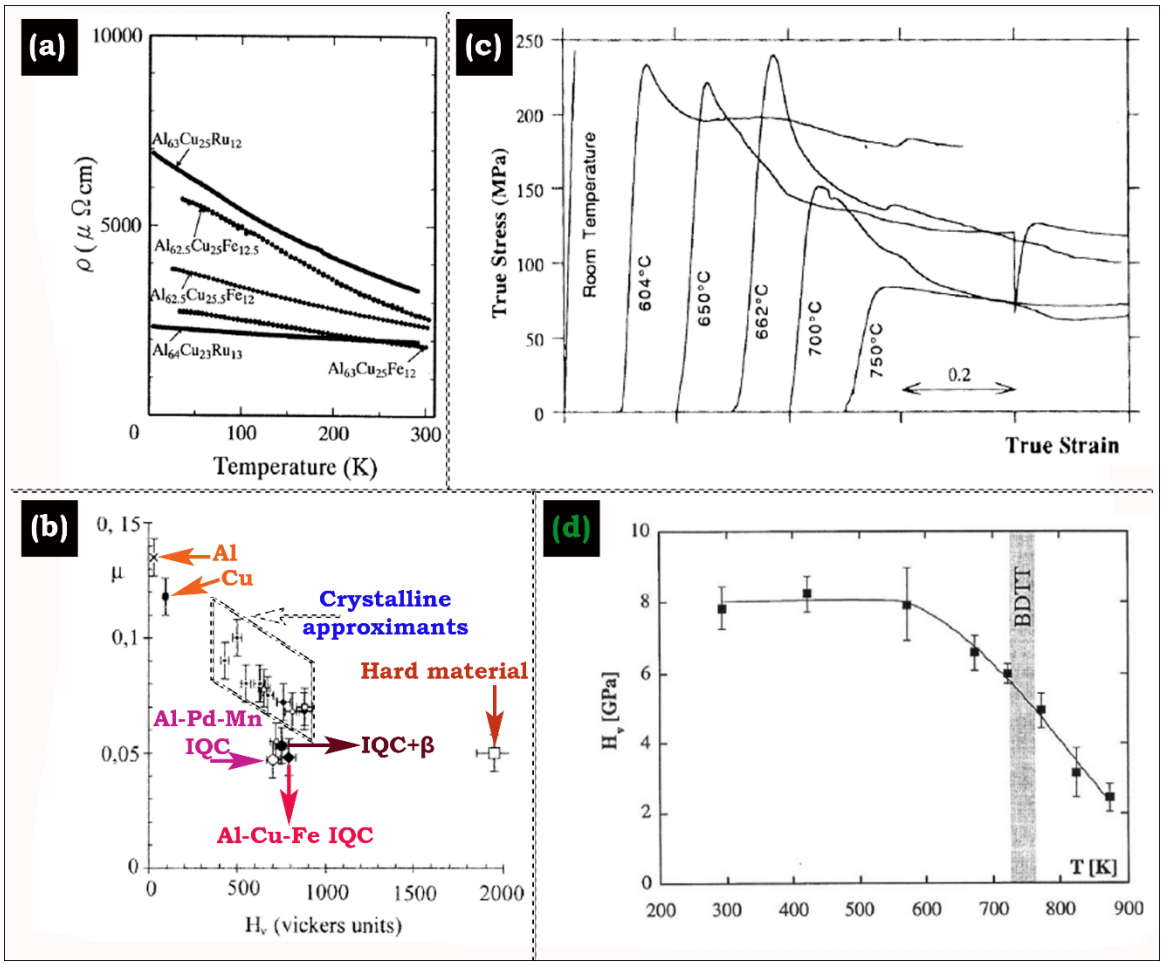

Figure 1. 3: (a) Temperature dependence of Al-Cu-Fe and Al-Cu-Ru quasicrystals [160]; (b) Co-efficient of friction observed for Al-based ternary quasicrystals during sliding scratch test [163]; (c) True stress-strain curve of Al-Cu-Fe IQC as a function of temperature [163]; (d) Vickers microhardness of Al-Cu-Fe IQC alloy as a function of temperature [164].

In the case of Al-Cu-Fe IQC alloys, no signature of magnetic behavior was observed [165] and $A_{65}Cu_{20}Fe_{15}$ (at %) retains its paramagnetic behavior down to 8 K (-265°C) [159]. In addition to the low electrical conductivity, the quasicrystalline materials show high solar absorbance (~90%) with low thermal emittance [166]. The thermal conductivity of quasicrystals is very similar to that of the oxides (also used as an efficient insulator) and lower than that of the crystalline counterpart [60]. The thermal conductivity of

quasicrystals increase with temperature upto 800 ℃ (1073K), however the increase in the thermal conductivity is not very significant [167]. Although the electrical conductivity of Al-Cu-Fe IQC alloys is dependent on the nominal composition, however, Bilusic et al. [161,168] have shown the thermal conductivity of $Al_{62}Cu_{25.5}Fe_{12.5}$ (at %), and $Al_{63}Cu_{25}Fe_{12}$ (at %) quasicrystals are the same.

1.5.2 Surface characteristics

The quasicrystalline materials without any crystalline phases have quasi-periodic arrangements of atoms even at their surface [58]. While studying quasicrystals surfaces, Jenks and Thiel [58] have observed the inter-atomic cluster's chemical bond strength to be significantly higher than that of the intra-atomic clusters. The surface of Al-Cu-Fe quasicrystals has screw dislocation as well as pentagonal pits, however, this is not true for the case of Al-Pd-Mn quasicrystals [169]. The surface energy of quasicrystals are relatively very low and usually lies in between that of the Teflon and steels. However, it is more closer to Teflon (only 25 to 30% less than quasicrystals) [154]. Therefore, quasicrystals surface energy behaves more or less like covalently bonded materials rather than the metal [58]. The friction coefficient for Al-Cu-Fe IQC alloys, crystalline approximant, and low carbon steel was 0.12, 0.14, and 0.4. The coefficient of friction for Al-Pd-Mn and Al-Cu-Fe IQC alloys, crystalline approximant phases, crystalline materials like Al and Cu, and hard materials like alumina hard Cr-steel are compared in Figure 1.3 (b). The friction coefficient for pure Al-Cu-Fe is almost half compared to that of the Al-Cu-Fe IQC with 5% cubic β-AlFe(Cu) alloy [154,163]. The wear resistance of quasicrystals is influenced by their hardness and brittleness [60]. The single Al-Cu-Fe IQC coating prepared by thermal spraying exhibits excellent abrasive wear resistance. However, the inherent room temperature brittleness may have a detrimental effect. Therefore, a small addition of

secondary phases like Sn, Fe-Al, etc. enhances the plastic flow of quasicrystals, increasing its abrasive wear resistance [90].

1.5.3 Mechanical properties

The crystalline material deformation depends on the dislocations that mediate the plastic flow and cause a strain field in one-dimensional space. Contrary to crystalline materials, quasicrystals possess strain fields in two direction-taking places in the perpendicular direction (Rper) and parallel direction (Rpar). The perpendicular and parallel elastic strain corresponds to the phason strain and the conventional elastic strains. Therefore, a perfect dislocation in quasicrystals can be physically understood only in higher dimensional space [60]. Thus, at low temperatures, the phason faults and low atomic diffusion restrict the dislocation movement, which is responsible for brittle fracture by an inter-granular process [170–172]. However, the quasicrystals show plasticity during deformation at high temperatures [173]. The Al-Cu-Fe quasicrystals also show very good high-temperature plasticity due to dislocation motion at elevated temperature [174–176]. Apart from the dislocation motions, the atomic diffusion over large distances may also be responsible for plastic deformation at elevated temperatures [172]. The twining phenomenon is also quite prevalent in Al-Cu-Fe quasicrystals during deformation at room temperature and high temperatures [177].

Figure 1.3 (c) represents the true stress-strain diagram of Al-Cu-Fe quasicrystals at room temperature to 750 °C (1073 K). It can be discerned that even at elevated temperature, the Al-Cu-Fe quasicrystals do not show any deformation hardening. Al-Cu-Fe quasicrystals microhardness has also demonstrated the temperature's dependence, as illustrated in Figure 1.3 (d). From the microhardness profile, it is clear that the Al-Cu-Fe quasicrystal retains its brittleness from room temperature to intermediate temperature [164]. However, further increasing temperature beyond 700 K reduces its hardness. This

is sometime referred to as brittle to ductile transition temperature (BDTT), also shown in the Figure 1.3 (d). These properties of Al-Cu-Fe quasicrystals make it a suitable candidate to be exploited for engineering applications.

1.6 Application of quasicrystals

1.6.1 Light absorption and sensors

The thin films of Al–Cu–Fe quasicrystals are candidate materials for selective absorbers in solar thermal applications due to their good solar absorbance (~90%) and optical properties. These solar absorbers of Al-Cu-Fe quasicrystals are already fabricated and can be used commercially [166]. The thermal conductivity of quasicrystals is similar to that of the oxides and lower than in crystalline materials [178]. Al-Cu-Fe quasicrystal's physical properties make them suitable for fabricating devices to detect heat flow [60]. The quasicrystals can also be used for thermos-electric power and as a device to detect IR radiations (Bolometers) [40].

1.6.2 Thermal barrier coatings

The lucrative mechanical and surface properties like high hardness accompanied by low friction and good wear resistance of Al-Cu-Fe quasicrystals justify their usage as a material for coating [86]. The quasicrystalline materials have been employed for coating the cylinder liners, pistons, and utensils used in day-to-day life [40].

1.6.3 Catalyst and hydrogen storage

A few quasicrystalline materials have shown exceptionally well catalytic application. The constituent elements used for fabricating quasicrystalline materials show good catalytic activity even independently in its elemental form, further justifying its usage for catalyst applications [179]. A P Tsai and co-workers make a significant contribution in understanding the steam forming capability of methanol ($CH_3OH+H_2O \rightarrow 3H_2+CO_2$) for

Al-Cu-Fe IQC alloys before and after leaching treatment [180–184]. Its nanostructuring can further tailor Al-Cu-Fe IQC alloy catalytic activity by making fine powders with high surface area [185]. The durability of Al–Cu–Fe IQC catalyst are more than that of the crystalline counterpart used under similar conditions. Recently, Yadav et al. [186,187] have shown the excellent hydrogen storage capacity of two-dimensional Al-based quasicrystalline alloys prepared by liquid exfoliation. In another study, Mishra et al. [188] have observed excellent catalytic activity for steam forming of methanol with an enhanced H_2 production rate of ~200 ml/g.min. The Ti-Zr-Ni-based quasicrystals belonging to the Bergman type of cluster have very appreciable hydrogen storage capacity and can be compared to metal hydrides. In the case of Ti-Zr-Ni quasicrystal, the protons can occupy the interstitial sites, and it has a total of storing hydrogen atom up to 2.5 wt% [40,189].

1.6.4 Strengthening of alloys

The quasicrystalline precipitates/ reinforcement incorporated by in-situ or ex-situ methods enhance alloys and metal matrix composites strength. The Sandvik steel has commercialized a special class of maraging steel with excellent mechanical properties possessing fine distribution of icosahedral phases [40]. Similarly, the Al matrix composite can be strengthened by in-situ and ex-situ reinforcement of these Al-based quasicrystals [60].

1.7 High entropy alloys

In 2004, Cantor et al. [2] and Yeh et al. [3] independently reported HEAs concept by alloying multi-principal elements. The investigation made by Cantor et al. [2] studied the alloying behavior of 16 to 20 elements in equiatomic proportion. They discerned the formation of two to three phases, contradicting the concept of Gibbs' phase rule. Further from their study, they have distinguished the formation of a single-phase FCC solid solution

for equiatomic CoCrFeMnNi HEA, popularly known as Cantor alloy. At the same time, Yeh et al. [3] independently observed the formation of single-phase solid solutions in many other multi-principal alloys. They further termed these multi-principal alloys as high-entropy alloys. HEAs inception brought a paradigm shift in the alloy design and development strategies breaking many conventional alloy development concepts.

The multi-principal alloy having entropy of mixing greater than 1.5R and having five or more alloying elements addition in between 5–35 at% was deemed the necessary criteria for forming HEAs. The formation of single-phase solid solution in HEAs can be related to one of the core effects, i.e., high-entropy effect, sluggish diffusion, severe lattice distortion, and cocktail effect. The high entropy effect of multi-principal elements stabilizes the disordered solid solution phase [190–192]. The HEAs having five or more alloying elements exhibit sluggish diffusion [190–192] due to decrement in the diffusion coefficient of elements, and the difference in the atomic sizes of elements in HEAs imparts severe lattice distortion in the alloys. It was observed that, with the increasing number of elements in HEA, the diffusion coefficient seemed to decrease [193]. However, non-sluggish diffusion was observed in some of the HEAs [190–193].

In a recent review, Miracle et al. [194] have classified the HEAs into seven alloy families, namely 3d transition metal HEAs, refractory metal HEAs, light metal HEAs, lanthanide (4f) transition metal HEAs, HEAs brasses and bronzes, precious metal HEAs and interstitial compound (boride, carbide, and nitride) HEAs. In another review, Steurer [195] studied the entire gamut of HEA reported till 2020. They observed that only 80 HEA composition shows the formation of single-phase solid solution.

The concept of high entropy alloys has also significantly evolved in the past two decades with the inception of near-equiatomic or non-equiatomic HEAs [196–198]. This class of HEAs usually has one or two principal alloying elements in the range of 30 to 45

at% and exhibits far superior properties than the equiatomic HEAs. The two popular classes of near or non-equiatomic HEAs contain Fe or Al as the primary alloying elements and are sometimes termed as Fe-based [196–198] or Al-based HEAs [199–208], respectively. Apart from these near/ non-equiatomic HEAs, a few recent studies have suggested the formation of single phase high entropy Laves intermetallics [209,210]. The HEAs compositions having a combination of Cantor alloy and Al have been studied extensively. However, there is a lot of scopes for exploring non-equiatomic Al-based HEAs for potential high-temperature applications. These properties of non-equiatomic HEAs make them candidate materials for coating applications as well as reinforcement in MMCs.

1.8 Aluminium based metal matrix composites

The quest for designing load-bearing structural materials with high strength to weight ratio has led to the development of metal matrix composites (MMCs) with superior physical and mechanical properties [211–216]. Among the different types of MMCs, the more widely used matrix includes aluminum alloys. Aluminum matrix composite (AMCs) are of significant interest in producing lightweight components that can replace high-density steel or cast iron parts. The AMCs are conventionally reinforced with ceramic particulate reinforcement, i.e., carbides, nitrides, and oxides with high strength and modulus of elasticity and thermal stability at higher temperatures [213,217]. The lack of bonding at the interface between the Al matrix and the ceramic particulates leads to the incoherency between the matrix and reinforcement, acting as a point of stress concentration for generation and propagation of crack [218]. The exorbitant cost involved in producing ceramic reinforcement like SiC, etc., is almost two to four times more than the price of Al and its alloys [219–221]. Apart from the cost economics involved, the low toughness, high wear of tools, and recycling of these classes of AMCs are extremely challenging [219–221].

A paradigm shift in the design philosophy of AMCs came after the discovery of Carbon Nano-tubes (CNTs) in the year 1991 [222]. Many researchers throughout the world started exploiting the possibility of using CNTs as reinforcement in AMCs due to their high modulus of elasticity (~ 1 TPa) and high tensile strength (≥ 30 GPa) [223]. However, the Vander Waals forces of attraction between the CNTs leads to its agglomeration in AMCs. To overcome the problem associated with agglomeration and homogenous distribution of CNTs in AMCs, many researchers have suggested high energy ball milling method for a homogenous distribution of CNTs [224,225]. Ball-milling techniques followed by hot-consolidation processes such as spark plasma sintering, spark plasma extrusion, hot-extrusion, and hot-rolling have generally been utilized to develop AMCs containing CNTs [222,226–231]. Esawi et al. [232] have demonstrated that the aluminum matrix composite reinforced by 5 wt.% CNTs showed around two times higher hardness value. Furthermore, the AMCs are reinforced by 2 wt.% CNTs, which was fabricated by a powder metallurgy route followed by annealing, shows 350 MPa in tensile strength and 8% in tensile elongation to failure [233]. Although CNTs may be homogenously distributed by the HEBM method, the ball-milling process induces undesirable defect structures in the CNTs [234,235]. Further, the AMCs reinforced with CNTs through stir cast techniques and consolidated by SPS, hot pressing, etc., above 500 °C (773 K) encounter the additional problem of deleterious formation Al_4C_3 intermetallic phases at the interface of Al matrix and CNT reinforcements [222,229,233,236,237].

For overcoming the shortcomings associated with AMCs reinforced with ceramic particles and CNTs, many researchers have demonstrated the incorporation of unconventional reinforcement in the AMCs for tailoring the interfaces of the matrix and reinforcement during fabrication. The widely used unconventional reinforcement materials in AMCs were industrial waste products [238], intermetallics [239–246], metallic glasses

[247,248,257–259,249–256], quasicrystalline materials [219,260–268], and high-entropy alloys [269–278]. In the investigation, Basariya et al. [238] have successfully demonstrated the fabrication of AA 6082 Al matrix composite reinforced with garnet. They have observed the nanostructured Al matrix due to the hard reinforcement particles used in the AMCs. In the recent past, considerable efforts were made to study the effect of glassy reinforcement particles in the AMCs. Khoramkhorshid et al. [279] have reinforced $Al_{84}Gd_6Ni_7Co_3$ glassy particles in 1050 Al alloys through accumulative roll bonding. After ARB of these composite for nine (09) passes, it was observed that the tensile strength and microhardness increase considerably to ~ 210 MPa and 85 HV respectively. In another investigation, Yang et al. [280] have fabricated 2024 Al alloy with $Al_{84}Ni_{8.4}Y_{4.8}La_{1.8}Co_1$ glassy reinforcement particles through hot pressing at 798 K. The enhancement in the tensile strength of AMCs with 20, 40, and 60 vol% of glassy reinforcement were reported to be ~ 545, 627 and 735 MPa respectively. Recently, Rashid and Scudino have reported the generation of harmonic structure in the AMCs reinforced with Fe_3Al intermetallic particles [245,281]. They have indicated that the formation of Al_5Fe_2 intermetallic at the interface of the Al matrix reinforced with Fe_3Al particles are subjected to hot pressing followed by hot extrusion. These composite bimodal and heterogeneous structure enhances the strength ~ 2 times compared to that of the unreinforced Al matrix. Similarly, many investigators and co-workers have made considerable efforts to study the effect of Al-based quasicrystalline and high-entropy alloys (HEAs) reinforcement in the AMCs. Among the available Al-based quasicrystalline alloys, the ternary Al-Cu-Fe quasicrystalline alloys are most popular due to non-toxicity, wide availability, and cost-effectiveness of the constituent elements [60,282].

1.8.1 AMCs reinforced with quasicrystals

The surge in overcoming the low interfacial strength and enormous problem associated with recycling AMCs reinforced with ceramic particulates led the researcher to design and develop AMCs reinforced with Al-based quasicrystals [219,260–268]. In the past three decades, considerable efforts were made to understand the structure and microstructure of quasicrystals. However, little has been done to explore the potential application of quasicrystals as reinforcement in MMCs. The initial study by Tsai and co-workers [283] in establishing the high-temperature strength of Al-Pd-Mn envisaged quasicrystal utility for dispersion strengthening quasicrystals. The noble idea for designing AMCs with Al-based icosahedral quasicrystals came from the early work of Tsai et al. [283] in the year 1993. They have reinforced pure Al matrix with 25 vol % of Al-Cu-Fe IQC and studied its effect on the strengthening behavior of AMCs [283]. They have hot pressed the Al-IQC composite at 673 K and 823 K. The IQC phase was stable up to 623 K, while at 823 K, the IQC particles transformed to ω-Al_7Cu_2Fe phase. However, on the transformation of IQC to ω-phase in AMCs, the hardness significantly reduces to 0.6 GPa from 1.2 GPa. After an initial attempt for designing ex-situ Al-IQC composite, the thrust was given for developing high strength Al alloys having in-situ formation quasicrystalline particles by Inoue and Kimura [284–286]. They have developed in-situ Al matrix composite falling into three broad categories having, i.e., high tensile strength (800 MPa), high elongation, and high strength at elevated temperatures. Based on the applicability of these in-situ AMCs, the composition of the same was adjusted to achieve the desired properties. For designing Al alloys with high tensile strength, an alloy with composition of $Al_{93.5}Cr_3Ce_1Co_{1.5}M$ (where M = Ti, Mn, Fe, Co, Ni, Cu, Zr or Mo) was chosen. They have also attempted to design in-situ AMCs for applicability at elevated temperature with

nominal composition of $Al_{84.2}Fe_7Cr_{6.3}Ti_{2.5}$ (at%). The tensile fracture strength of this alloy at 573 K was ≥320-350 MPa.

After the initial success in designing the ex-situ and in-situ AMCs with IQC particles have brought an impetus for developing such AMCs by various equilibrium and non-equilibrium processing routes. The early contribution made by Fleury et al. [287–289] is worth mentioning for fabricating AMCs with scalable size by liquid metallurgy route. The mechanical properties of AMCs manufactured by liquid metallurgy routes are poorer than powder metallurgy routes. The IQC alloy used in the study by Fleury et al. [287–289] was prepared by gas atomization and have a minor amount of β, τ, λ, and θ phases along with a major icosahedral phase. The as-cast Al-IQC composite has phases of β, τ, λ, ω and θ phases along with a major icosahedral phase. However, the θ-Al_2Cu phases appearing as satellite particles on the gas atomized IQC phase does not exist in the as-cast composite sample. This confirms the precipitation of θ-phase during melting and solidification of Al-IQC composite. Additionally, the precipitation of ω-phase was also observed, and these help in the precipitation hardening of such composites. They have further discussed the effect of the Al matrix on the strengthening of AMCs reinforced with quasicrystals. For studying the effect of matrix materials, they have used $Al_{96}Cu_4$ (at %) reinforced with the gas atomized Al-Cu-Fe quasicrystals [287]. They have reported a significant improvement in the mechanical properties of $Al_{96}Cu_4$ (at %) Al alloy reinforced with IQC reinforcement. The details of the mechanical properties of both the kind of AMCs are mentioned in Table 1.3.

The compressive strength for Al alloy containing 5 vol% of IQC reinforcement is more than that for the pure Al containing 20 vol% of IQC. In this study, Fleury et al. [287] have fabricated Al-IQC composite by induction melting instead of the conventional casting route employed in the previous investigation and have observed an increase in the

compressive strength of the composite. The inquiry by Fleury et al. [287] reported the presence of minor crystalline phases in the reinforcement. To understand the effect of pure IQC phase on the strengthening of AMCs during processing by liquid metallurgy route, Lee et al. [290] have heat-treated the gas atomized Al-Cu-Fe alloys at 750 ℃ for 3 h to obtain IQC phase without any minor fraction of crystalline phases. Further, the Al-Cu-Fe IQC alloys were coated with a 5 μm Ni layer to avoid the Al matrix's reaction during melting and solidification. They have observed that the formation of crystalline phases (i.e., θ, τ and ω) and the parent IQC phase, as it was inevitable, even restrict the formation of crystalline phases even after Ni coating of quasicrystals [290]. However, due to large undercooling, the formation of λ and β-phases are surpassed. They have compared their finding with those of the commercially available AMCs reinforced with 10 vol% of Al_2O_3 or SiC. They observed the strength of AMCs having the same fraction of quasicrystalline reinforcement has significantly higher strength than AMCs with ceramic particulates.

Simultaneously, Shurack et al. [263,291–293] made a significant contribution in understanding the microstructure, phases formed and strength of in-situ and ex-situ AMCs reinforced with Al-Mn-Ce, Al-Pd-Mn and Al-Cu-Fe quasicrystals. They have fabricated the in-situ Al/Al-Mn-Ce and Al/Al-Pd-Mn AMCs by die casting method at a moderate cooling rate in a copper mold [291]. Further, they have extended the concept of in-situ Al/Al-Mn-Ce and Al/Al-Cu-Fe composite through mechanical milling followed by hot pressing and hot extrusion [293]. The strength of the in-situ composite can be tuned in the range of 442 MPa to 762 MPa based on the adjustment in the chemical composition of Al-Mn-Ce and Al-Cu-Fe quasicrystal [293]. After the initial attempt to fabricate Al/Al-Cu-Fe composite by Tsai et al. [283], Tang and co-workers revolutionized the concept for processing AMCs having quasicrystalline reinforcement by vacuum quasi-static forging [294,295] and vacuum hot pressing techniques [219,220,296]. They have synthesized Al-

Cu-Fe quasicrystals by inert gas atomization and commercially available atomization techniques and studied its effect on the microstructure and mechanical properties of Al-IQC composite. They have observed superior properties for composite consisting of IQC alloy processed by inert gas atomization techniques, as shown in the Table 1.3.

The contribution made by Kenzari et al. [264,297] for understanding the effect of Al-Cu-Fe-B quasicrystals reinforced AMCs are worth mentioning. They have reported that the pre-oxidation treatment of AlCuFeB IQC significantly reduces the Al diffusion kinetics from Al matrix to IQC particles up to 823 K to enhance the structural stability of Al-Cu-Fe quasicrystalline particles in the Al matrix. The pre-oxidation treatment for a longer duration has a deleterious effect on the strengthening behavior of Al-IQC composite (Table 1.3). Although, with the help of pre-oxidation treatment, Al-Cu-Fe quasicrystals can retain their identity up to 823 K. However its effect on mechanical properties was not very encouraging.

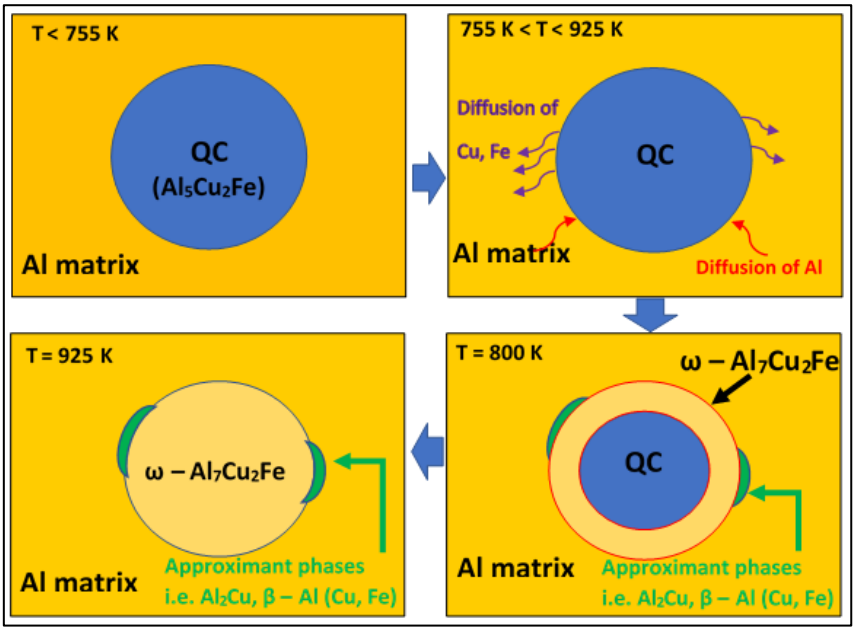

Figure 1. 4: Evolution and stability of phases at the interfaces of Al–IQC composite during hot pressing [298].

In recent years, Lityńska-Dobrzyńska, Coddet and co-workers have made a significant contribution in studying the interfaces of Al/ Al-Cu-Fe QC AMCs [298–305]. The Al-based metal matrix composites with high strength combined with considerable plastic deformation have been synthesized by powder metallurgy route through the consolidation of elemental Al powder blended with different amounts of quasicrystalline reinforcements. The detailed investigation of the sequence of phase evolution during sintering of Al-IQC composite can be schematically shown in Figure 1.4.

Table 1. 3: Mechanical properties of AMCs reinforced with Al-based quasicrystals.

Matrix	Reinforcement	Vol %	YS (MPa)	UTS (MPa)	ε_f (%)	Hardness	Processing and fabrication	Ref.
Al 1070	$Al_{65}Cu_{23}Fe_{12}$	0	-	111	35	50 HV	Multi-pass Friction stir processing	[306]
		4	-	173	32	79 HV		
		6	-	189	30	86 HV		
		8	-	206	25	91 HV		
ZL101 A	$Al_{63}Cu_{23}Fe_9Cr_3$	0 wt%	-	220			Stir casting followed by aging	[307]
		1.33	-	240				
		5.30	-	279				
		9.29	-	292				
ZL101 A	$Al_{72}Ni_{13}Co_{10}Mn_5$	0 wt%	-	281	5%		Stir casting followed by aging	[308]
		1	-	313	7%			
		4	-	338	8%			
		7	-	298	4%			
Al	$Al_{70}Cu_{10}Cr_{10}Fe_{10}$	0	91				Mechanical milling+SPS at 450 °C for 10 min	[309]
		20	299					
Al	Al-Cu-Li 2050 alloy (3.4 wt% Cu, 1.2 wt% Li, Al- 95.4 wt%)	5	105	119	12.5	3.91 GPa	Microwave sintering (550°C)+hot extrusion at 350°C with reduction	[310]
		5	114	128	10.8			
		10	122	152	8.3			
		15	138	167	6.4	7.27 GPa		

							ratio of 20.25:1	
Al	$Al_{70}Cu_{10}Cr_{20}Fe_{10}$	0	Wear rate: 1.39×10^{-3} $mm^3/N{\cdot}m$				Mechanical milling + SPS at 450℃ for 10 min	[311]
		20	Wear rate: 2.19 × 10−4 $mm^3/N{\cdot}m$					
6061 Al	$Al_{62.5}Cu_{25}Fe_{12.5}$	0	155		63		Mechanical milling + hot pressing at 400℃ for 1 h	[312]
		20	330		55			
		40	407		25			
Al	$Al_{65}Cu_{20}Fe_{10}Cr_5$	30 wt%		292	8	180 HV	Mechanical milling + selective laser melting	[313]
		30+ HT @480℃		291	8.7	160 HV		
		30+ HT @540℃		266	6.6	158 HV		
		30+ HT @570℃		278	6.9	155 HV		
Al	Al-Cu-Fe QC	40		450	4.3		Mechanical milling + SPS at 823 K for 2 min	[314]
		HT 473 K		350	4.8			
		HT 523 K		200	5.1			
		HT 573 K		180	5.5			
		HT 723 K		50	7.5			
6061 substrate	Al-Cr-Mn-Co-Zr gas atomized IQC alloy	35				301 HV	VIM + gas atomization + cold spraying	[262]
Al	B_4C+ $Al_{62.5}Cu_{25}Fe_{12.5}$	12 wt% (B_4	102	151		35	Mechanical milling + Sintering at	[315]

		C +IQC)					400°C for 1hr at 10°C/min	
		12 wt% B_4C	79	124		28		
		12 wt% IQC	90	130		44		
Al	$Al_{65}Cu_{20}Fe_{15}$	20	155	215	-	60 HV	Mechanical milling + cold pressing + hot extrusion at 420 ℃; addition aging for Al2124 at 191℃ for 9 h	[316]
	$Al_{70.5}Pd_{21}Mn_{8.5}$	20	141	-	-	-		
Al2124	$Al_{65}Cu_{20}Fe_{15}$	20	561	655	6	180HV		
	$Al_{70.5}Pd_{21}Mn_{8.5}$	20	535	725	7.5	190HV		
Al	$Al_{87.5}Cr_{6.7}Mn_3Co_{2.4}Zr_{0.3}$		690		6		VIM + gas atomization + pressure less sintering + hot forging at 350 ℃	[317]
Al	$Al_{62}Cu_{25.5}Fe_{12.5}$	0	101	-	>40	39 HV	Gas atomization of IQC + mechanical milling of Al-IQC composite + hot pressing at 673 K for 10 min	[301]
		20	114	195	25	64 HV		
		40	138	221	22	83 HV		
		60	307	366	07	173 HV		
Al	$Al_{62}Cu_{25.5}Fe_{12.5}$	0	101	-	>50	39 HV	Melt spinning of IQC + mechanical milling + hot pressing at 673 K for 10 min	[298]
		20	176	-	>50	72 HV		
		40	268	397	10	101 HV		
		60	-	545	-	180 HV		
Al-1Si-7Mg	$Al_{65}Cu_{25}Fe_{12}$+ SiC	1.2 wt% IQC		285		80 HB	Mechanical milling of	[318]

		+ 1.2wt% SiC					IQC & SiC + induction melting	
Al	40 vol% $Al_{62.5}Cu_{25}Fe_{12.5}$	HE-693 K	195				Mechanical milling + hot pressing at 637 K for 10 min + hot extrusion (HE) at 4:1	[319]
		HE-743 K	265					
		HE-753 K	325					
		HE-773 K	390					
		HE-848 K	400					
Al-12.6%Si	$Al_{63}Cu_{25}Fe_{12}$	0 wt%		250	8.5	87 HB	Stir casting + Cu mould pouring	[320]
		3		270	8.9	96 HB		
		6		310	7.7	102 HB		
		9		280	4.1	122 HB		
Al	25% $Al_{65}Cu_{20}Fe_{15}$	0% Mg	527	850	23		Mechanical milling + pressure-less sintering at 450℃ + HE at 540℃ (25:1)	[321]
		4% Mg	660	895	7			
		8% Mg	1113	1155	5.5			
Al-7%Si	$Al_{63}Cu_{25}Fe_{12}$	0	Impact energy absorbed: 7.0 $J.cm^{-2}$			56 HB	Stir – casting	[322]
		3	Impact energy absorbed: 10.0 $J.cm^{-2}$			66 HB		
		6	Impact energy absorbed: 11.4 $J.cm^{-2}$			69 HB		
		9	Impact energy absorbed: 6.5 $J.cm^{-2}$			85 HB		
Al	$Al_{59.2}Cu_{25.5}Fe_{12.3}B_3$	0	129	98	26.8		Mechanical milling + cold isostatic pressing +	[323]
		3	98	47	14.3			
		6	129	57	5.5			

							hot extrusion at 500 °C with extrusion ratio of 6.25:1	
A356 Al	$Al_{72}Ni_{12}Co_{16}$	0 wt%	93	164	4.0	58	Al-Ni-Co d-QC prepared by VIM + Stir – casting	[324]
		2.5	102	173	3.8	70		
		5	108	170	3.6	72		
		7.5	110	155	3.2	72		
		10	115	147	2.5	70		
Al	Al-Cu-Fe IQC	0	50	100			Hot pressing of Al-IQC composite powder at 673 K and 823 K	[325]
		40+ HP 673 K	180	210				
		40+ HP 823 K	330	410				
Al	$Al_{63.5}Cu_{24.0}Fe_{12.5}$	40+ RT		190			Hot isostatic pressing at 673 K followed by compressive testing from 293 – 823 K	[326]
		393 K		157				
		423 K		140				
		493 K		130				
		593 K		115				
		693 K		75				
		823 K		20				
Al	$Al_{59}Cu_{25.5}Fe_{12.3}B_3$	0	104			41 HB	Gas atomization of IQC + cold isostatic pressing at 1.6 GPa + Sintering at 32MPa for 3.5 h	[297]
	Non- Oxidized $Al_{59}Cu_{25.5}Fe_{12.3}B_3$	15	159			67 HB		
	Oxidized $Al_{59}Cu_{25.5}Fe_{12.3}B_3$ (10 h)	15	127			50 HB		
	Oxidized $Al_{59}Cu_{25.5}Fe_{12.3}B_3$ (100 h)	15	72			40 HB		
	Non Oxidized $Al_{59}Cu_{25.5}Fe_{12.3}B_3$	30	251			100 HB		

	Oxidized $Al_{59}Cu_{25.5}Fe_{12.3}B_3$ (75 h)	30	183			70 HB		
	Non Oxidized $Al_{59}Cu_{25.5}Fe_{12.3}B_3$	60	405			184 HB		
Al	$Al_{72}Ni_{12}Co_{16}$	0	37	64	30		Stir -casting	[266]
		7	49	83	3			
		10	52	87	2			
		15	63	104	<1			
Al	$Al_{86}Mn_{12}Ce_2$	80		565-830	3	110-438 HV	VAR of IQC + Mechanical milling + Hot-extruded at 623 K with 12:5 ratio	[291]
	$Al_{92}Mn_6Ce_2$	55		600	11	322 HV		
	$Al_{91}Mn_7Fe_2$	45		455	6			
Al	$Al_{63}Cu_{25}Fe_{12}$	GFF -15	193	154			Gas atomization of IQC alloy and Al + cold isostatic pressing at 200 MPa + hot forging at 550°C for 10 min at 635 MPa; (GFF & AFF refers to synthesis of alloy by inert and commercial techniques respectively)	[294, 295]
		GFF -20	135	222				
		GFF -30	191	238				
		AFF -15	135	176				
		AFF -20	154	178				
		AFF -30	199	233				
Al	$Al_{62}Cu_{26}Fe_{12}$	0	96	100			Gas atomization of IQC alloy + Induction melting of Al-IQC composite	[288]
		5	144	320				
		10	211	510				
		15	178	-				
		20	227	590				
Al	$Al_{62}Cu_{26}Fe_{12}$	5	92	320			Gas atomization of IQC alloy + Stir casting of	[290]
		10	139	510				
		15	171	-				
		20	188	590				

							Al-IQC composite	
Al	$Al_{62}Cu_{26}Fe_{12}$	0	45	59			Gas atomization of IQC alloy + Stir casting of Al-IQC composite	[287]
		5	135	144				
		10	207	195				
		15	177	206				
		20	242	240				
$Al_{96}Cu_4$	$Al_{62}Cu_{26}Fe_{12}$	0	110	118				
		5	247	268				
Al matrix	B_4C + $Al_{62.5}Cu_{25}Fe_{12.5}$	0	8.1	20.8		19.8 HV	Mechanical milling + hot pressing at 400℃ for 1 h	[327]
		3+3	28.9	59.6		24.5 HV		
	B_4C	6	10.6	45.3		37.5		
	$Al_{62.5}Cu_{25}Fe_{12.5}$	6	13.5	48.6		29.0		
Al	$Al_{63}Cu_{25}Fe_{12}$	40	363	26.2	25.8		IQC prepared by mechanical alloying + Mechanical milling of Al-IQC + hot extrusion at 623 K with 6:1 ratio	[263]
		50	419	15.6	14.7			
		60	524	10.3	9.2			
		80	660	3.1	1.8			

Recently, Khan et al. [315,327] have made concentrated efforts in understanding the hybridization of Al-IQC composites by the addition of B_4C ceramic particulates. The hybrid composite has higher strength due to the formation of ω-phase, which restricts the formation of the Al_3BC phase after sintering. In most of the studies, the Al-IQC composites are fabricated either by liquid metallurgy routes, hot pressing, hot isostatic pressing, etc. However, many researchers and investigators have used other non-equilibrium techniques such as ultrasonic impact peening [267,328–330], spark plasma sintering [309,311,314], microwave sintering [310], and selective laser melting [313,331,332] for fabricating Al-IQC composites. The details of the various non-equilibrium processing routes employed

for the fabrication of Al-IQC composite are elaborated in Table 1.3. The effect processing routes on the mechanical properties are also briefly described in Table 1.3.

1.8.2 AMCs reinforced with high-entropy alloys

The concept of reinforcing high entropy alloys (HEAs) as a reinforcement in the MMCs have evolved in past five years [269–278]. The single solid solution HEAs have good high strength at room temperature and high temperature, high oxidation resistance, high hardness, high fracture toughness, good corrosion resistance [190–192]. These exciting properties of HEAs make them a suitable reinforcement in MMCs. The exciting properties of HEAs can be exploited for the strengthening of Al matrix composites. The nature of bonding in the Al matrix and HEAs particles in AMCs is expected to be coherent as discerned for Al-IQC composites cases. This class of AMCs also offers the formation of an interfacial or transitional layer, which enhances its load-bearing capacity by inhibiting the formation of cracks at the interfaces due to the de-bonding of matrix and reinforcement particles. The formation of the transition layer between the matrix and HEA reinforcement further improves the wettability [269]. In 2014, Wang et al. [269] took initiative to reinforce the 2024 Al matrix with non-equiatomic $FeNiCrCoAl_3$ HEA alloy particles having a single BCC phase. They have processed the AMCs through mechanical milling followed by got extrusion at a temperature of 773 K. They have reported high strength ~710 MPa for 2024 Al matrix reinforced with HEA particles. In an investigation, Kumar et al. [333] reinforced HEA particles in 2024 Al matrix through sit casting with appreciable mechanical properties. These initial study paved the concept for AMCs reinforced with HEA particles. To date a few investigation have been conducted to study the AMCs reinforced with HEA particles through pressure-less sintering [334], hot pressing/ hot extrusion [274], spark plasma sintering [335], stir-casting [333], additive manufacturing

[272], and friction stir processing (FSP) [336]. The details of the processing routes and the mechanical properties of the processed AMCs are mentioned in Table 1.4.

Table 1. 4: Mechanical properties of AMCs reinforced with HEA particulates processed through various techniques.

Matrix	Reinforce-ment	Vol %	Processing route	Mechanical Properties			Ref.
				YS (MPa)	UTS (MPa)	ε_f (%)	
2024 Al	HEA-$FeNiCrCoAl_3$ (BCC)	0	Mechanical milling + Hot extrusion at 773 K and 500 MPa; *(raw 2024 Al) + 80%(MA alloyed 40%HEA + 2024Al)	300	-	-	[269]
		40		500	-	-	
		20*		710	-	-	
2024 Al	HEA- Al–20Cu–10Mg	0 wt%	Stir casting	207	330	16.5	[333]
		5		311	401	12.5	
		10		380	493	10.8	
		15		405	563	8.6	
$Al_{65}Cu_{16.5}Ti_{18.5}$	HEA-$Al_{0.6}CoCrFeNi$ (FCC+BCC)	0	Gas atomization of HEA + mechanical milling of matrix + blending of composite + SPS at 823 K and 400 MPa	1700	-	-	[337]
		50		3120	-	-	
AA5083 Al	HEA-CoCrFeNi (FCC + minor BCC phase)	0	Without processing	180	300	12	[272]
		0	Friction stir processing at a spindle speed of 800 r.p.m, 8 kN force and 25 s friction time	210	325	10	
		12		280	395	5	
7075 Al	5% ($CoNiFeAl_{0.4}Ti_{0.6}Cr_{0.5}$) + 40% (SiC)	45%	MM of HEA + blending of HEA & SiC for 24 h + Squeeze casting of Al-HEA/SiC at 100 MPa	662	712	0.82	[273]

	SiC (45%)	45%		540	596	0.65	
6061 Al	HEA-$CoNiFeAl_{0.4}Ti_{0.6}Cr_{0.5}$	0	MM of HEA + MM of Al-HEA + Hot pressing at 490℃, 120 MPa + Hot extrusion at 450℃ with 10:1; solution strengthening at 510℃ + ageing at 175℃ for 5 h	238	-	-	[274]
		7.5 (10h)		-	378	8.4	
		7.5 (40h)		348	385	-	
Al	HEA-AlCoCrFeNi	5*	VIM & gas atomization of HEA + Al-HEA MM + SPS at 60MPa and 10 min (T=540℃*; 560℃**; 580℃**)	96	-	-	[275]
		5**		105	-	-	
		5***		137	-	-	
2024 Al	HEA-$CoNiFeCrAl_{0.6}Ti_{0.4}$	0	MM of HEA + MM of Al-HEA + Hot pressing at 490℃, 120 MPa, 0.5 h + Hot extrusion at 450℃ with 10:1; *solution strengthening at 480℃ + ageing at 195℃ for 6 h	307	-	-	[276]
		7.5*		419	-	8	
		15		-	-	-	
		30		-	-	-	
2024 Al	HEA-CoCrFeMnNi	0	MM of Al-HEA + SPS at 823 K, 40 MPa	80 HV			[335]
		7		135 HV			
AA5083 Al	HEA-$Al_{0.8}CoCrFeNi$	0	Friction stir processing at a spindle speed of 800 r.p.m with 4 no's of pass	141	304	24.3	[336]
		3.8		200	371	18.8	
Al	HEA-CuZrNiAlTiW	0	Mechanical alloying of HEA + MM of Al-HEA + SPS at 773 K, 80 MPa, 30 min	39	98	15.1	[338]
		10		258	344	7.2	
		20		-	544	6.5	
		30		-	270	3.0	
5083 Al	HEA-AlCoCrFeNi	10	Gas atomization of HEA + submerged friction stir processing at a spindle speed of 800 r.p.m, 40 mm/min with 5 no's of pass	145	-	-	[339]

Al-Mg alloy	HEA-AlCoCrFeNi	0	submerged friction stir processing	184	327	-	[340]
		10		219	401	-	
5052Al	HEA-Al0.6CoCrFeNi	7	MM + hot pressing at 823 K, 30 MPa, 6 min + heat treatment at 350℃, 500℃, 600℃ for 24 h; HT at 500℃ for 12 & 48 h	HT 12 h: Hardness=1.81 GPa HT 48 h: Hardness-1.61 GPa			[341]
Al	HEA-AlCoCrCuFe	15	MM of Al-HEA + cold pressing at 600 MPa + pressureless sintering at 580℃ for 2 h	-	-	-	[334]

1.9 Powder Metallurgy

The art and science of producing powder materials and their densification into desired shapes is the sole goal of powder metallurgy [342,343]. The powder metallurgical techniques have the potential for developing high performance materials by tailoring its microstructures and mechanical properties with intricate shapes and sizes [342,343]. The powder metallurgical techniques also offer fabrication of materials practically impossible through conventional routes. For example, the synthesis of single-phase solid solution is not possible in the MgAlSiCrFe HEA system having a different melting point and diffusion coefficient alloying elements. However, Singh et al. [344] have reported major BCC phase formation with a minor fraction of retained Si processed through high-energy ball milling. The powder metallurgical processing usually consists of two main steps (i) powder production and (ii) powder consolidation through various equilibrium and non-equilibrium routes.

1.9.1 Powder production

The modernization of processing techniques enables the synthesis of the wide range of powder materials [342]. The processing techniques renaissance has aimed to develop

and produce metal powders with desired quality, low operational cost, and meeting the specified properties required for the end product [342,343]. The vividly used techniques for producing metal powders include gas and water atomization, ball milling, electrolysis, and reduction of oxides through various chemical routes [342]. The desirable physical and chemical properties of metal powder and the cost involved in its production suitable manufacturing techniques are selected [342]. It may be understood with the end-product obtained through atomization techniques and electrolytic methods. While the atomization techniques are useful for producing powders of different materials with suitable size and shape, disintegrating the molten metal stream is forced through a nozzle [342,343]. On the other hand, chemical and electrolytic methods may produce high purity metal powders [342,343].

The most popular and cost-effective top-down method for producing powder materials involves ball milling. Ball milling techniques can circumvent the restriction imposed for alloying through conventional processing methods. These techniques can also produce composites and nanocomposites with a uniform distribution of reinforcement, which is seldom possible by conventional solidification and rapid solidification routes [345–347]. The ball milling is usually used for producing nanostructured alloys and composite of hard metals and oxides. The ball milling techniques can also be employed for secondary processing of powder materials produced through atomization techniques, chemical and electrolytic methods [345–347]. The HEBM techniques are used for making Al-Cu-Fe-based quasicrystalline and 6082 Al matrix nanocomposites in the present work. In light of the importance of high energy ball milling in the current work, a brief description of the method and process variables usually considered during ball milling is explained in the below-mentioned sections.

1.9.2 Ball milling

The ball milling techniques impart severe plastic deformation to powders along with fracturing and cold welding of milled particles. The fracturing and cold welding of milled powders are due to powder particles entrapment between the colliding balls during ball milling [345–347]. The ball milling of powder particles can be accomplished with various mills, i.e., attrition mills, shaker mills, planetary mills, and vibratory mills [346,348]. For milling, the powder materials and milling balls are loaded into the container (steel or tungsten carbide) of the desired size, usually known as vials. The properties such as particles size achieved, degree of disorder or amorphization, grain refinement, the extent of alloying, etc. depends upon the various parameters such as type of mills, the ball to powder ratio, milling media, milling atmosphere, milling temperature, duration of milling, the material of the milling vials and balls [349]. In the past three decades, ball milling has evolved from a technique for just particle size reduction to its present-day status for designing and developing technologically necessary materials [346,348]. Among the various ball mills available high energy planetary ball mills are used for synthesising and processing all kind materials [346,348]. The term planetary ball mills are coined for these kind of mills due to the planetary motion of the vials containing the powders [349]. The local temperature also rises during high energy planetary ball milling due to high intensity of impacts received by the powder particles entrapped between the colliding balls [349]. It is usually observed that the rise in temperature during high energy planetary ball milling varies in the range of 100 – 200 K [350].

1.9.3 Powder consolidation

The consolidation of powders into the bulk form of desired shape and size is paramount in the powder metallurgical processing of materials [351]. During the consolidation of powder materials, a bulk product with a close net or near net shape product

with the desired density is produced [351]. The powder can be consolidated using various pressure-less sintering techniques like conventional sintering, microwave sintering, selective laser melting (SLM), etc. or through non-equilibrium sintering with the application of pressure like SPS, HP, HE, and HIP etc. For proper densification of powder materials, non-equilibrium processing routes such as SPS, HP, and HE are widely used today [342,351].

The consolidation of powder particles through SPS and HP is almost the same. However, the mechanism of the sintering of the particles is a bit different [352]. In both cases, the powder material is placed in the die of either graphite or any other suitable material based on the applied pressure or temperature chosen. In the case of SPS, the pulsed direct current with the application of pressure is used to generate the spark between the powder particles due to the generation of plasma. The plasma generated during SPS vaporizes the impurity due to a localized increase in the temperatures and further leads to the melting of the powder particles in contact. However, due to the pulsed direct current, the on-cycle helps in the melting of the particles, and during the off-cycle, a vacuum is created between them. This led to the formation of a neck between the powder particles during the SPS process [352]. In contrast to this, the mechanism of heating is different in the case of HP. During HP, external heating sources such as induction or resistance heating are employed, while SPS pulsed direct current being used.

Compared to hot pressing, SPS techniques are more advantageous as they inhibit the grain coarsening due to the different sintering modes. SPS is a very effective technique for sintering dissimilar materials and in particular, this is very effective for sintering composite materials with uniform distribution of reinforcements [352]. Apart from this high heating rate during SPS, it helps achieve a consolidated product comparatively less

time. Further, the microstructure and density of the SPSed sample can be tuned by altering the process parameters.

1.10 Motivation

The depletion of natural energy resources and geo-political concerns for reducing the global carbon footprint has incentivized the search for alternative energy resources and technologically advanced materials with high strength to weight ratio. The ever increasing demand for technologically superior materials has brought a paradigm shift in the alloy design and development strategies. This surge in the development of new materials has led to the discovery of quasicrystals [1], bulk metallic glasses [353], and high-entropy alloys [193] among other exotic materials. In 1984, the first report on quasicrystals had forced the scientific community to re-define conventional crystallographic concepts. Similarly, another breakthrough was evidenced in 2004, with HEAs discovery surpassing all the traditional notions of alloy development. The high strength and hardness, good wear resistance, low thermal conductivity make these candidate materials for many technological importance applications. These properties of quasicrystal and non-equiatomic HEA make them a suitable material for coating and dispersion strengthening of MMCs. However, the inherent room temperature brittleness of quasicrystals and non-equiatomic Al based HEAs restrict their direct implication as a structural materials in engineering applications. For overcoming the limitation of room temperature brittleness, these materials can be toughened by either nanostructuring or embedding soft phases into the quasicrystals.

There have been many attempts to toughening the quasicrystalline matrix either by nanostructuring or by embedding the soft phases like Sn into the quasicrystalline matrix. Most of the studies have concentrated their efforts on dispersing the soft phases through liquid metallurgy routes. The melting and solidification techniques impose the additional

challenge for uniform distribution of Sn in the quasicrystalline matrix. To overcome this limitation, mechanical milling can be employed for the homogenous distribution of Sn in the quasicrystalline matrix nanocomposites. The exciting properties of Al-Cu-Fe quasicrystals can be used for dispersion strengthening of Al matrix composites. The earlier attempts for the synthesis of Al-IQC composite through liquid metallurgy routes impose additional challenges of retaining the IQC phase, which usually transforms to ω-phase. The best and cost-effective method for synthesis of Al-based nanocomposite reinforced with IQC and non-equiatomic HEA is high energy planetary ball milling. To overcome the formation of ω-phase during the synthesis of the Al-IQC composite, it consolidates them through SPS by adjusting the parameters to overcome the Al-Cu-Fe IQC to ω-phase. Therefore, the present work has made very systematic efforts to understand the effect of Sn addition into Al-Cu-Fe IQC alloy, Al-Cu-Fe quasicrystal, and non-equiatomic HEAs into AA 6082 Al matrix processed through mechanical milling and non-equilibrium sintering (in particular SPS).

1.11 Objective of the thesis

The primary objective of the present work is to understand the phase evolution, thermal stability, and indentation behavior of mechanically milled nanocomposite powders of IQC-Sn, Al-IQC, and Al-HEA. Further, it will be interesting to study the toughening behavior of IQC-Sn composite and interfaces of Al-IQC composites consolidated through various non-equilibrium sintering routes. The broad objectives are mentioned as follows:

- Synthesis of Al-Cu-Fe IQC alloy, non-equiatomic $Al_{40}(SiCrMnFeNiCu)_{60}$ HEA.
- Structural evolution of Sn reinforced Al-Cu-Fe IQC matrix nanocomposite during mechanical milling.
- Thermal stability of Sn reinforced Al-Cu-Fe IQC matrix nanocomposite.

- Consolidation of IQC-Sn nanocomposite powder by SPS and HP.
- Indentation and toughening behavior of IQC-Sn nanocomposite powder and consolidated bulk compact.
- Structural evolution of Al-Cu-Fe IQC alloy reinforced Al matrix and non-equiatomic $Al_{40}(SiCrMnFeNiCu)_{60}$ HEA reinforced Al matrix nanocomposite by MM.
- Thermal stability of non-equiatomic $Al_{40}(SiCrMnFeNiCu)_{60}$ HEA reinforced Al matrix composites.
- Non-equilibrium processing through SPS of Al-IQC nanocomposite powder.
- Strengthening and toughening of bulk Al-IQC and Al-HEA composite.